EJNMMI Research
a SpringerOpen Journal

ORIGINAL RESEARCH Open Access

Pilot study of PET imaging of ^{124}I-iodoazomycin galactopyranoside (IAZGP), a putative hypoxia imaging agent, in patients with colorectal cancer and head and neck cancer

Joseph A O'Donoghue[1*], José G Guillem[2], Heiko Schöder[3], Nancy Y Lee[4], Chaitanya R Divgi[5], Jeannine A Ruby[2], John L Humm[1,3], Steven A Lee-Kong[6], Eva M Burnazi[3], Shangde Cai[3], Sean D Carlin[3], Tobias Leibold[7], Pat B Zanzonico[1,3] and C Clifton Ling[1]

Abstract

Background: Hypoxia within solid tumors confers radiation resistance and a poorer prognosis. ^{124}I-iodoazomycin galactopyranoside (^{124}I-IAZGP) has shown promise as a hypoxia radiotracer in animal models. We performed a clinical study to evaluate the safety, biodistribution, and imaging characteristics of ^{124}I-IAZGP in patients with advanced colorectal cancer and head and neck cancer using serial positron emission tomography (PET) imaging.

Methods: Ten patients underwent serial whole-torso (head/neck to pelvis) PET imaging together with multiple whole-body counts and blood sampling. These data were used to generate absorbed dose estimates to normal tissues for ^{124}I-IAZGP. Tumors were scored as either positive or negative for ^{124}I-IAZGP uptake.

Results: There were no clinical toxicities or adverse effects associated with ^{124}I-IAZGP administration. Clearance from the whole body and blood was rapid, primarily via the urinary tract, with no focal uptake in any parenchymal organ. The tissues receiving the highest absorbed doses were the mucosal walls of the urinary bladder and the intestinal tract, in particular the lower large intestine. All ^{124}I-IAZGP PET scans were interpreted as negative for tumor uptake.

Conclusions: It is safe to administer ^{124}I-IAZGP to human subjects. However, there was insufficient tumor uptake to support a clinical role for ^{124}I-IAZGP PET in colorectal cancer and head and neck cancer patients.

Trial registration: ClinicalTrials.gov NCT00588276

Keywords: Hypoxia, Iodine-124, IAZGP, PET imaging, 2-Nitroimidazole, Radiation dosimetry, Head and neck cancer, Colorectal cancer

Background

There is substantial evidence that tumor hypoxia is an important indicator of clinical prognosis for human cancer. The hypoxic tumor phenotype is complex; its various aspects include reduced sensitivity to low LET radiation, differential patterns of gene expression, enhanced angiogenesis, and an increased propensity to metastatic dissemination [1-8]. Although a full understanding of all the implications of hypoxia has yet to be achieved, relatively simple polarographic probe measurements in accessible tumors typically show a difference in survival between patients with hypoxic tumors and those with non-hypoxic tumors [9-11]. It follows that a non-invasive imaging method, even if it could provide only the same information as polarographic probes, could potentially help predict tumor behavior and enable individualized courses of treatment to be designed on a rational basis.

Positron emission tomography (PET) using hypoxia-selective radiotracers has been proposed as a non-invasive method of visualizing hypoxia within solid tumors.

* Correspondence: odonoghj@mskcc.org
[1]Department of Medical Physics, Memorial Sloan-Kettering Cancer Center, New York, NY 10065, USA
Full list of author information is available at the end of the article

However, the optimal radiotracer has yet to be identified. Typical candidate radiotracers for hypoxia imaging are radiolabeled small molecules that freely diffuse into (and out of) cells but are differentially metabolized in regions of low pO_2. In hypoxic cells, the molecules are irreversibly reduced and their radiolabeled metabolites bind to macromolecules, resulting in intracellular trapping. Conversely, in non-hypoxic cells, the molecules remain operationally intact and diffuse back out again. Achieving a hypoxia imaging differential requires that the radiolabeled tracer accumulates in sufficient quantity in hypoxic regions while clearing relatively quickly from normoxic regions.

However, hypoxia in tumors is, at least partly, a consequence of a dysregulated and chaotic vascular network leading to an imbalance between oxygen supply and demand. It is likely that this dysfunctional vasculature will also impose some restriction on the delivery of molecular tracers for hypoxia imaging. In contrast, the supply of such tracers to better-vascularized non-hypoxic tumor regions is likely to be greater. Accordingly, the intratumoral distribution of a hypoxia tracer would be expected to undergo a kinetic evolution from an initial state, where it is dominated by vascular supply (higher tracer concentrations in non-hypoxic regions), toward a final state, where it is dominated by the accumulation of trapped metabolites (higher concentrations in hypoxic regions). The hypoxia selectivity of such tracers would thus be expected to increase with time.

There are, however, practical limits to the length of time that is available between tracer administration and imaging. The most commonly used 2-nitroimidazole-based hypoxia radiotracers (^{18}F-fluoromisonidazole [12,13] (^{18}F-FMISO), ^{18}F-fluoro-azomycin-arabinoside [14,15] (^{18}F-FAZA), ^{18}F-2-(2-nitro-1H-imidazol-1-yl)-*N*-(2,2,3,3,3-pentafluoropropyl)-acetamide [16,17] (^{18}F-EF5), ^{18}F-fluoro-erythronitroimidazole [18,19] (^{18}F-FETNIM)) are all labeled with the positron-emitting radionuclide fluorine-18 (^{18}F), and its relatively short (110 min) half-life limits the time for PET image acquisition to a maximum of approximately 3 h post-injection. This may be insufficient to produce a static image that reflects only tumor hypoxia. In principle, the longer (12.6 h) half-life of ^{64}Cu allows later imaging times for the candidate hypoxia radiotracer ^{64}copper-diacetyl-bis(N4)-methylthiosemicarbazone (^{64}Cu-ATSM). However, current clinical imaging studies of ^{64}Cu-ATSM typically involve early (<1 h post-injection) imaging [20,21], partly due to historical experience with positron-emitting isotopes of Cu with shorter half-lives (e.g., ^{60}Cu = 24 min, ^{62}Cu = 10 min) [22,23].

As an alternative to static imaging, kinetic analysis of dynamically acquired PET data has been proposed for assessment of tumor hypoxia [24,25]. This enables generation of parametric images of uptake rate constants or time-activity curve slopes which may, due to the deconvolution of 'supply' (i.e., vascular functionality) and 'demand' (i.e., hypoxic bioreduction), provide a more accurate representation of tumor hypoxia. This approach, however, has problems of its own related to the long and complex imaging protocols required, image noise, and the accurate determination of arterial input function.

Based on the foregoing considerations, we decided to investigate the use of a long-lived radiolabeled 2-nitroimidazole compound, ^{124}I-iodoazomycin galactopyranoside (^{124}I-IAZGP) to enable late static imaging of tumor hypoxia. The positron-emitting radionuclide ^{124}I has a half-life of 4.2 days enabling, in principle, imaging at times in excess of 24 h post-injection. Additionally, a series of *in vitro* studies with tumor cells in culture and *in vivo* studies in murine xenograft models provided support for the hypothesis that ^{124}I-IAZGP might be a superior radiotracer for non-invasive imaging of tumor hypoxia using late PET imaging [26-28]. In order to study ^{124}I-IAZGP in human subjects, an investigational new drug application (IND 72,013) was submitted to the US Food and Drug Administration (FDA). Subsequently, we performed a clinical study to evaluate the safety, biodistribution, and imaging characteristics of ^{124}I-IAZGP in a group of patients with advanced colorectal cancer and head and neck cancer using serial PET imaging. We now present the results of this clinical study.

Methods

Clinical study with ^{124}I-IAZGP

Under the auspices of a protocol approved by the Institutional Review Board and an Investigational New Drug application approved by the FDA, ten patients (eight males, two females) with either colorectal or head and neck cancer were intravenously administered 1 mg of IAZGP labeled with ^{124}I after having provided informed consent (trial registration ID NCT00588276). Patients underwent serial whole-torso (head/neck to pelvis) PET imaging together with multiple whole-body counts and blood draws. Potential thyroid uptake of ^{124}I was blocked by oral administration of potassium iodide (ten drops of SSKI) initiated 2 days before and continued for 2 days after administration of the radiotracer.

Radiotracer

A single lot of cold precursor stable iodoazomycin galactopyranoside (IAZGP also known as 1-(6-deoxy-6-iodo-β-D-galactopyranosyl)-2-nitroimidazole), synthesized in accordance with cGMP principles by Dr. R.F. Schneider as described previously [26], was used for all clinical studies. IAZGP was radiolabeled with ^{124}I produced on an in-house cyclotron (TR19/9, EBCO Technologies, Inc., Vancouver, Canada) by exchange labeling and purified by AgCl-treated celite/anion exchange chromatography as described previously [26]. The radiolabeled drug product

was formulated as 1.0 mg IAZGP in sterile physiological saline (pH 6 to 8). Specific activity was nominally 148 MBq/mg (4 mCi/mg) with a radiochemical purity >95%.

PET imaging

The initial plan was to perform serial whole-torso ^{124}I-IAZGP PET scans in a series of ten patients with each patient administered 1 mg of IAZGP labeled with 148 MBq (4 mCi) of ^{124}I. Following discussions with the FDA, the first three patients were administered a reduced activity (nominally 111 MBq:3 mCi) of ^{124}I, and a provisional analysis was performed before further patient accrual. The provisional analysis led us to modify the imaging scheme for the remaining patients in the study. Specifically, the first three patients were imaged on three to four occasions at nominal times of 3, 18 to 24, and 48 h following injection of 111 MBq of ^{124}I-IAZGP (imaging scheme A). The seven remaining patients were imaged on three occasions at nominal times of 3, 6 to 8, and 24 h following injection of 148 MBq of ^{124}I-IAZGP (imaging scheme B). For the first three patients, at least one scan was a PET/computer tomography (CT) scan (GE Discovery LS, Waukesha, WI, USA) with the remaining scans as PET only (GE Advance). For the subsequent seven patients, all scans were PET/CT scans (GE Discovery LS, n = 1; GE Discovery ST, n = 1; GE Discovery STE, n = 5). Torso (head/neck to pelvis) PET scans, typically comprising 6 to 7 bed positions, were acquired in two-dimensional (2D) mode with attenuation, scatter, and other standard corrections applied to yield quantitative (Bq/ml) PET images. ^{124}I-IAZGP PET scans were interpreted by a board-certified nuclear medicine physician with lesions, identified from contemporaneous ^{18}F-fluorodeoxyglucose (FDG) PET scans, scored as either positive or negative for ^{124}I-IAZGP uptake.

Absorbed dose estimates for ^{124}I-IAZGP

Absorbed doses to normal tissues for ^{124}I-IAZGP were estimated using measured whole-body and blood clearance data, together with uptake data derived from region-of-interest (ROI) analysis of the serial PET scans. Dose estimates were generated using organ-level internal dose assessment/exponential modeling (OLINDA/EXM) [29] for either standard 'Adult Male' or 'Adult Female' model as appropriate. The input data consisted of cumulative activity per unit administered activity (also known as residence time) for ^{124}I-IAZGP for a set of source organs, as discussed in detail below.

Whole-body and blood clearance

Whole-body clearance was determined by serial measurements of count rate by a NaI(Tl) scintillation probe. Duplicate anterior and posterior measurements were made at fixed geometry, and background-corrected geometric mean values were used for clearance curve fitting. Probe measurements were made immediately post-administration before first voiding, after each voiding over a period of approximately 3 h post-administration, and subsequently at the times of PET imaging. The median number of whole-body count rate measurements was 7 (range, 5 to 10). Count rates were normalized to the value immediately post-administration (taken as 100%) to yield relative retained activities (%).

A median of 10 (range, 9 to 10) venous blood samples (approximately 5 ml) were drawn at nominal times of 5, 15, 30, and 60 min after administration of ^{124}I-IAZGP, and before and after each scan up to the nominal 24-h time point. Aliquots (500 μl) of blood or serum were counted in duplicate in a NaI(Tl) gamma well-type detector (Wallac Wizard 1480 automatic gamma counter, PerkinElmer, Waltham, MA, USA) calibrated for ^{124}I, the net count rates converted to activities and the results expressed in terms of percentage of the injected dose per unit volume (%ID/l). It was verified, using multiple patient samples, that whole blood and serum activity concentrations were equivalent.

Bi-exponential functions were fitted to the whole-body and blood clearance data using the software application SAAM II (University of Washington, Seattle, WA, USA).

Parenchymal organs (liver, kidneys, spleen, lung, and thyroid)

Multiple ROIs were drawn on several transverse CT slices for each of the liver, kidneys, spleen, lung, and thyroid and copy/pasted onto the corresponding PET slices. The average activity concentrations in each ROI (Bq/ml) were recorded, and the overall average values were derived for each organ. The total activity in each organ was estimated by multiplying the activity concentration by standard male or female organ masses (i.e., the masses used in OLINDA/EXM). The density of all organs was assumed to be 1 g/ml, except for the lung which was assumed to be 0.3 g/ml. Total cumulated activities in the organs were estimated by trapezoidal integration of the activity-time curve and expressed as cumulative activity per unit administered activity (h) for input into OLINDA/EXM.

Gastrointestinal tract

The fraction of activity clearing via the gut was estimated from the PET scans acquired the day after administration of ^{124}I-IAZGP. It was assumed that all activity clearing via this route would be present in the gut at this time, based on respective nominal transit times of 4, 13, and 24 h for the small, upper large, and lower large intestines [30]. PET images were reformatted to generate summed coronal and sagittal projections, and ROIs were drawn to encompass the entire visible intestine; ROI

counts were then expressed as a fraction of the total counts in the patient. The fraction of administered ^{124}I-IAZGP present in the intestine was estimated by multiplying the average of the coronal and sagittal count fractions by the decay-corrected whole-body activity at the time of scanning (derived from the whole-body clearance curve). This was then used as input to the ICRP 30 gastrointestinal (GI) module of OLINDA/EXM to yield cumulative activity per unit administered activity for the small, upper large, and lower large intestines.

Cardiac contents and red marrow

Estimates of cumulative activity per unit administered activity for cardiac contents and the red marrow were derived from the blood clearance curve. The volume of the cardiac contents was taken as 510 ml for males and 370 ml for females, based on standard values [31]. Red marrow mass was taken as 1,120 g for males and 1,300 g for females, corresponding to the values used in OLINDA/EXM. Given the equivalent activity concentrations between whole blood and serum and the implication of unhindered trans-plasma membrane transport of ^{124}I-IAZGP, the conservative assumption was made that the activity concentration in the red marrow was equal to that in the whole blood.

Urinary bladder

It was assumed that any material not cleared via the GI tract was cleared via the urinary bladder. As this corresponded to the majority of administered ^{124}I-IAZGP, the conservative assumption was made that the pharmacokinetics of urinary clearance was identical to the bi-exponential whole-body clearance, and these parameters (fractions and biological half-times) were used in the voiding bladder model of OLINDA/EXM.

Results and discussion

Results

PET imaging with ^{124}I-IAZGP

Ten patients completed the study, including five patients with colorectal cancer, four patients with head and neck cancer, and one patient with pseudomyxoma peritonei (Table 1). No adverse effects related to the administration of ^{124}I-IAZGP were observed in any patient. ^{18}F-FDG PET scans acquired shortly before ^{124}I-IAZGP administration indicated FDG-avid disease in all patients. However, all ^{124}I-IAZGP PET scans were interpreted as negative, i.e., there was no differential or focal uptake of ^{124}I-IAZGP in any disease site at any time. Figure 1 shows an example of a patient with FDG-avid primary rectal cancer with widespread FDG-avid liver metastases, indicating the absence of ^{124}I-IAZGP uptake in any sites of disease. Figure 2 shows a patient with head and neck cancer where, again, ^{124}I-IAZGP uptake is not observed in FDG-avid disease. Additionally, as illustrated in both figures, there was no focal ^{124}I-IAZGP uptake in any parenchymal organ in any patient at any time. Physiologic/excreted ^{124}I was seen in the urinary and GI tracts and the salivary glands.

Biokinetics of ^{124}I-IAZGP

Clearance of ^{124}I-IAZGP from the whole body and blood was very rapid and was adequately described by bi-exponential clearance curves of the form $A(t) = A_1 \exp(-a_1 t) + A_2 \exp(-a_2 t)$. The best-fit parameters for the whole body indicated that, on average, two thirds of the activity cleared with an effective half-time of 1 h and the remaining one third with an effective half-time of 11 h (Table 2). For blood, the average effective $T_{1/2}$ values for the faster and slower clearance components were 0.24 and 5.2 h, respectively (Table 2). Biological clearance

Table 1 Patient characteristics

Patient	Tumor site	Histologic subtype	Differentiation	TNM	IAZGP (MBq)	Imaging scheme	IAZGP uptake	Neoadjuvant therapy	Response (%)
1	Pseudomyxoma peritonei	Mucinous adenocarcinoma	Moderate	N/A	116	*A*	(–)	None	N/A
2	Tonsil	Squamous	Moderate to poor	$cT_1N_2M_0$	108	*A*	(–)	Radiation	NED
3	Tonsil	Squamous	Poor	$cT_4N_2M_0$	59	*A*	(–)	CRT	NED
4	Tongue	Squamous	Poor	$cT_1N_1M_0$	160	*B*	(–)	CRT	NED
5	Rectum	Mucinous adenocarcinoma	Poor	$pT_4N_2M_0$	148	*B*	(–)	CRT	95%
6	Rectum	Adenocarcinoma	Moderate	$pT_3N_0M_1$	141	*B*	(–)	Chemotherapy	50%
7	Rectum	Adenocarcinoma	Moderate	$pT_3N_0M_0$	150	*B*	(–)	CRT	60%
8	Rectum	Adenocarcinoma	Moderate	cT_4NxM_1	159	*B*	(–)	Chemotherapy	Progression
9	Supraglottic larynx	Squamous	Moderate	$cT_3N_2M_0$	157	*B*	(–)	CRT	NED
10	Sigmoid	Adenocarcinoma	Moderate	$cTxN_2M_1$	159	*B*	(–)	Chemotherapy	Progression

Serial whole-body, blood, and PET data were acquired for patients 1 to 10. Post-imaging clinical management and response are also shown. *CRT* chemoradiotherapy, *NED* no evidence of disease. Imaging schemes: *A* = 3, 18 to 24, and 48 h post ^{124}I-IAZGP injection; *B* = 3, 6 to 8, and 24 h post ^{124}I-IAZGP injection.

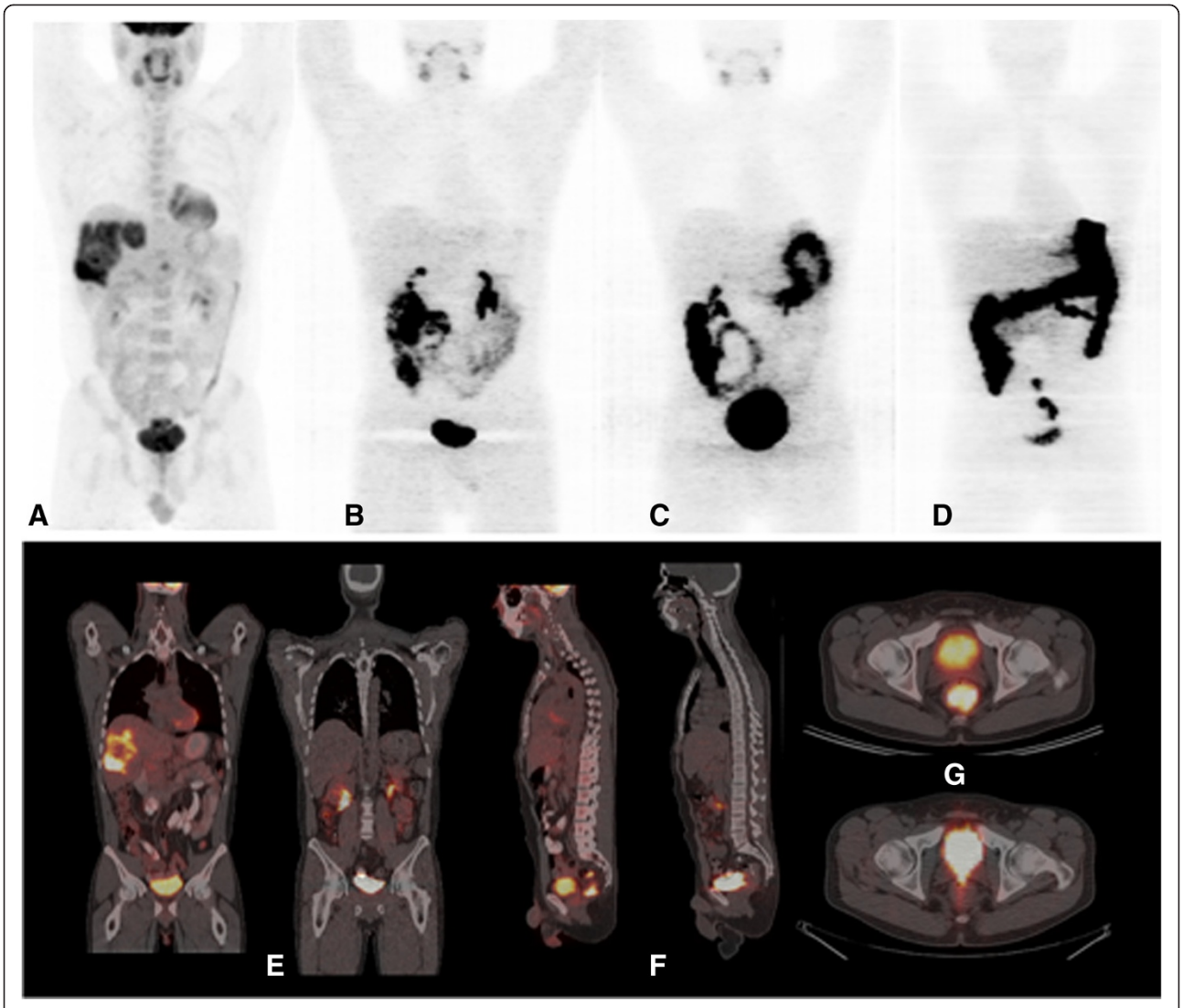

Figure 1 PET/CT images of ^{18}F-FDG and ^{124}I-IAZGP in a rectal cancer patient. (**A** to **D**) Coronal maximum intensity projection PET images of ^{18}F-FDG acquired 3 days before ^{124}I-IAZGP administration (**A**) and ^{124}I-IAZGP acquired at 3 h (**B**), 6 h (**C**), and 25 h (**D**) post-administration in a patient with primary rectal cancer with liver metastases. (**E** to **G**) Cross-sectional fused PET/CT images of the same patient comparing ^{18}F-FDG (**E** and **F** left, **G** top) with ^{124}I-IAZGP at 3 h (**E** and **F** right, **G** bottom). No evidence of ^{124}I-IAZGP uptake is seen in either FDG-avid primary or metastatic lesions. The ^{124}I-IAZGP MIP images (**B** to **D**) also illustrate the characteristic pattern of ^{124}I-IAZGP clearance, initially via the urinary tract with longer term excretion via the GI tract. Note that image intensities are not directly comparable as window levels were adjusted to maximize feature visibility.

was primarily via the urinary tract with urinary bladder and, to a lesser extent, renal components visible at early imaging times. At later times (approximately 24 h post-administration), a significant proportion (up to 50%) of total activity was visible in the intestines. However, by this time, the amount of activity present in the whole body was only a small fraction (<10%) of that administered. The fraction of ^{124}I-IAZGP clearing via the intestinal route was estimated to be, on average, 0.03 (range, 0.02 to 0.05) of that administered (Table 2).

Residence times and absorbed dose estimates for normal tissues

Table 3 shows the values of cumulated activity per unit administered activity (i.e., residence time) estimated for patients 1 to 10 as described in the 'Methods' section. The OLINDA/EXM-derived absorbed dose estimates based on these input data, together with the associated effective dose [32] values, are shown in Table 4. This indicates that the tissues receiving the highest absorbed doses were the mucosal walls of the urinary bladder and

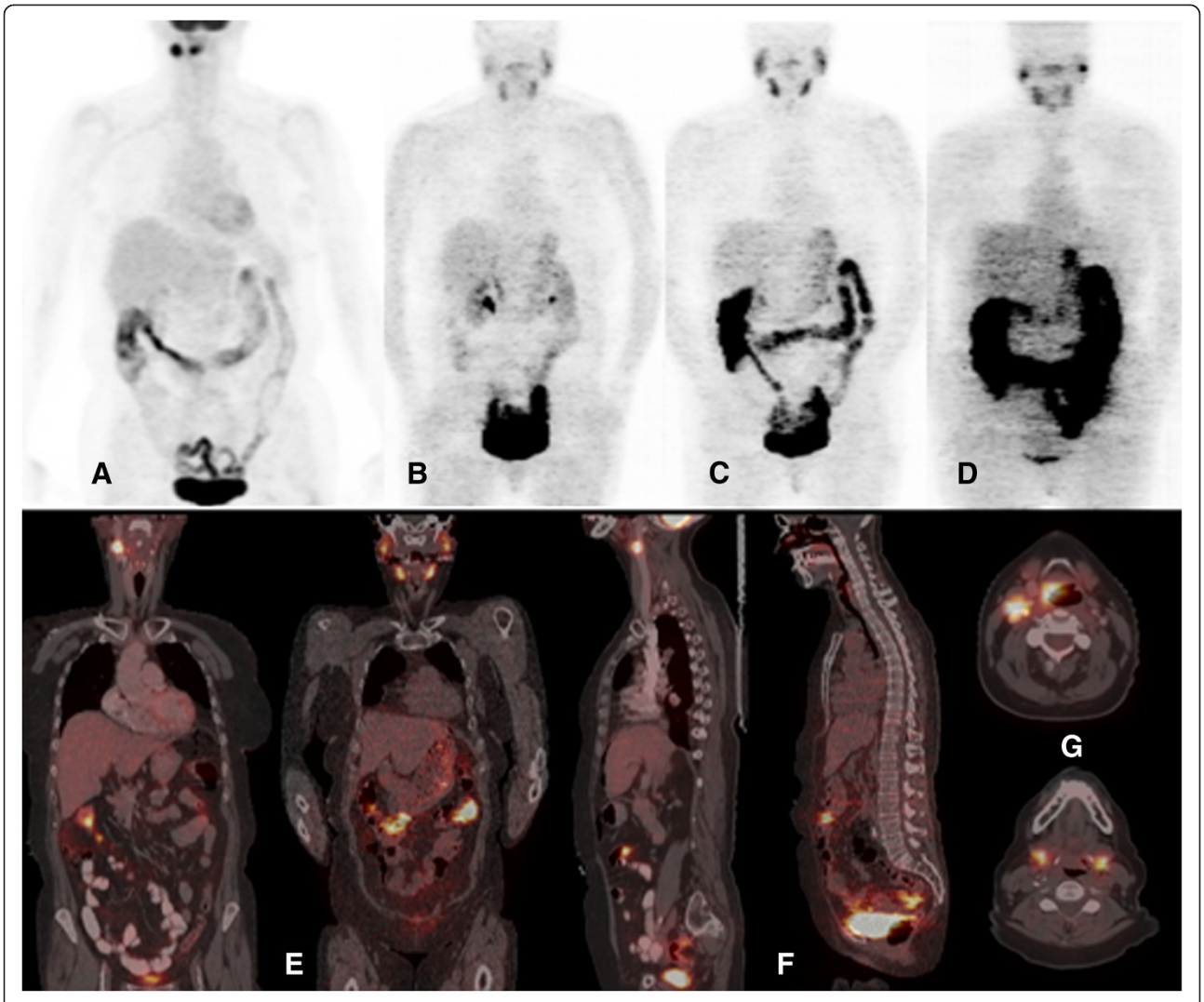

Figure 2 PET/CT images of ^{18}F-FDG and ^{124}I-IAZGP in a head and neck cancer patient. (**A** to **D**) Coronal maximum intensity projection PET images of ^{18}F-FDG acquired 3 days before ^{124}I-IAZGP administration (**A**) and ^{124}I-IAZGP acquired at 3 h (**B**), 6 h (**C**), and 27 h (**D**) post-administration in a patient with head and neck cancer. (**E** to **G**) Cross-sectional fused PET/CT images of the same patient comparing ^{18} F-FDG (**E** and **F** left, **G** top) with ^{124}I-IAZGP at 6 h (**E** and **F** right, **G** bottom). No evidence of ^{124}I-IAZGP uptake is seen in either the FDG-avid supraglottic larynx cancer or the approximately 2-cm lymph node. The clearance of ^{124}I-IAZGP is similar to that seen in Figure 1, with a symmetric distribution of physiologic ^{124}I in the salivary glands. Note that image intensities are not directly comparable and that the ^{18}F-FDG image was acquired in the radiotherapy treatment position with the patient in a facial mask.

the intestinal tract, in particular the lower large intestine. Average estimated absorbed doses to the bladder wall (0.27 to 0.69 mGy/MBq:1.0 to 2.5 cGy/mCi) were dependent on the assumed frequency of voiding. The average absorbed dose to the LLI wall was 0.35 mGy/MBq (1.3 cGy/mCi). The highest average absorbed dose estimate to the parenchymal organ was 0.056 mGy/MBq (0.21 cGy/mCi) to the kidney followed by 0.044 mGy/MBq (0.16 cGy/mCi) to the liver. The average absorbed dose estimate to the thyroid was 0.022 mGy/MBq (0.082 cGy/mCi). For an administration of the clinically envisaged activity of 148 MBq (4 mCi) of ^{124}I-IAZGP, the average absorbed dose to the parenchymal organs was estimated at 0.47 cGy with the kidney receiving an average absorbed dose of 0.83 cGy.

Discussion

This study was designed to evaluate the safety, biodistribution, and imaging characteristics of ^{124}I-IAZGP in human patients. In particular, the primary imaging function was to assess the time-dependent biodistribution of ^{124}I-IAZGP throughout the whole body, rather than its intratumoral distribution, and image acquisition parameters were, necessarily, suboptimal for this latter role. It is also important to note that, like other tumor hypoxia PET tracers, ^{124}I-IAZGP is not a tumor imaging agent *per se*,

Table 2 Kinetic clearance parameters for patients

Patient #	1	2	3	4	5	6	7	8	9	10	Mean	SD
WB A_1	0.67	0.89	0.86	0.70	0.80	0.50	0.67	0.28	0.71	0.67	0.67	0.18
WB a_1 (h^{-1})	0.29	0.24	0.38	1.11	0.45	2.10	0.53	0.89	0.52	0.98	0.75	0.56
WB A_2	0.33	0.11	0.14	0.30	0.20	0.50	0.33	0.72	0.29	0.33	0.33	0.18
WB a_2 (h^{-1})	0.06	0.02	0.03	0.06	0.05	0.09	0.08	0.08	0.06	0.10	0.06	0.03
Blood A_1 (%/l)	5.9	18.7	5.7	2.2	5.1	7.1	3.5	2.5	3.2	2.6	5.7	4.9
Blood a_1 (h^{-1})	5.1	6.5	5.8	0.8	1.3	5.6	0.7	1.4	0.8	1.0	2.9	2.5
Blood A_2 (%/l)	1.3	2.48	1.2	0.38	0.68	0.88	0.88	1.07	0.74	0.61	1.01	0.58
Blood a_2 (h^{-1})	0.12	0.12	0.13	0.08	0.07	0.45	0.07	0.10	0.09	0.12	0.13	0.11
Gut fraction	0.031	0.030	0.027	0.049	0.037	0.033	0.030	0.050	0.047	0.016	0.03	0.02

Whole-body and blood clearance data were fitted to bi-exponential functions viz $A(t) = A_1 \exp(-a_1 t) + A_2 \exp(-a_2 t)$, where t is time in hour. Gut fraction is the estimated fraction of ^{124}I-IAZGP present in the intestine at (nominally) 24 h after administration.

and its potential clinical role would be to characterize tumors that had been pre-identified by other means. Nevertheless, the fact that no differential uptake of ^{124}I-IAZGP was observed in any disease site must be considered disappointing. It is unlikely that this finding is due to the absence of tumor hypoxia in the study patients. For example, Figure 1 shows large volume FDG-avid, centrally cold liver metastases suggestive of significant central necrosis and thus likely to contain perinecrotic hypoxic regions.

There is a major discrepancy between the previous pre-clinical studies of ^{124}I-IAZGP, which demonstrated its ability to detect hypoxia in tumor cells both *in vitro* and in small animal models [27,28,33,34], and these clinical findings. One factor in this discrepancy may be related to the dilution effect when transitioning from a small animal to a human subject (in terms of both mg/kg and MBq/kg). Our pre-clinical studies used activities of approximately 16.7 MBq in 25-g mice [27] or approximately 18.5 MBq in 200-g rats [28], corresponding to approximately 100 to 700 MBq/kg. In contrast, patients in this study were injected with approximately 148 MBq corresponding to approximately 2 MBq/kg, a factor of 50 to 350 times less than the pre-clinical studies.

We hypothesized that the concentration of radioactivity in tumors might just be too low to be detected with the clinical PET scan parameters used. In order to address this, after the ten-patient imaging study was complete, we included one additional patient who was pre-scheduled for surgical resection of a sigmoid tumor. For this patient, approximately 300 MBq (8 mCi) ^{124}I-IAZGP was administered the day before surgery, clinical

Table 3 Cumulated activity per unit administered activity (residence time) in hours for patients 1 to 10

	Patient number										Mean	SD
	1	2	3	4	5	6	7	8	9	10		
Sex	M	M	M	M	M	M	M	M	F	F		
Heart contents	0.061	0.117	0.050	0.037	0.071	0.017	0.089	0.063	0.046	0.029	0.058	0.030
Kidneys	0.112	0.161	0.108	0.035	0.035	0.065	0.043	0.048	0.055	0.037	0.070	0.043
Liver	0.24	0.55	0.53	0.19	0.17	0.13	0.24	0.31	0.17	0.14	0.27	0.15
Lungs	0.068	0.148	0.089	0.058	0.052	0.046	0.074	0.106	0.062	0.046	0.075	0.032
Red marrow	0.13	0.26	0.11	0.08	0.16	0.04	0.19	0.14	0.16	0.10	0.14	0.06
Spleen	0.014	0.034	0.039	0.013	0.011	0.011	0.012	0.013	0.011	0.008	0.017	0.011
Thyroid	0.0011	0.0039	0.0012	0.0009	0.001	0.001	0.002	0.001	0.001	0.001	0.0014	0.001
LLI	0.56	0.54	0.49	0.90	0.62	0.60	0.25	0.93	0.86	0.19	0.59	0.25
SI	0.12	0.12	0.10	0.19	0.13	0.13	0.05	0.20	0.18	0.04	0.13	0.05
ULI	0.35	0.34	0.31	0.57	0.39	0.38	0.16	0.58	0.54	0.12	0.37	0.16
UB cont (1 h)	0.49	0.49	0.50	0.54	0.51	0.56	0.51	0.49	0.51	0.54	0.51	0.03
UB cont (2.5 h)	1.28	1.28	1.35	1.56	1.37	1.60	1.39	1.31	1.38	1.53	1.41	0.12
ROB (1 h)	6.35	6.20	4.84	3.49	4.41	4.14	4.16	6.40	4.21	3.14	4.73	1.19
ROB (2.5 h)	5.55	5.41	3.99	2.47	3.55	3.10	3.28	5.58	3.34	2.15	3.84	1.26

LLI lower large intestine, *SI* small intestine, *ULI* upper large intestine, UB cont (*t*), urinary bladder contents for a voiding interval of *t*; ROB (*t*), remainder of body for a bladder voiding interval of *t*.

Table 4 Estimated absorbed dose to normal tissues for ^{124}I-IAZGP

	Patient number										Mean	SD
	1	2	3	4	5	6	7	8	9	10		
Sex	M	M	M	M	M	M	M	M	F	F		
Adrenals	0.038	0.043	0.034	0.022	0.027	0.024	0.021	0.039	0.034	0.022	0.030	0.008
Brain	0.025	0.025	0.019	0.013	0.017	0.016	0.015	0.026	0.021	0.015	0.019	0.005
Breasts	0.024	0.025	0.020	0.013	0.017	0.015	0.015	0.025	0.021	0.014	0.019	0.005
Gallbladder wall	0.046	0.053	0.045	0.035	0.036	0.033	0.026	0.054	0.047	0.026	0.040	0.011
LLI wall	0.33	0.32	0.29	0.49	0.35	0.34	0.16	0.52	0.52	0.14	0.35	0.13
Small intestine	0.080	0.080	0.068	0.090	0.074	0.071	0.043	0.108	0.110	0.042	0.077	0.023
Stomach wall	0.039	0.041	0.033	0.027	0.029	0.027	0.023	0.043	0.038	0.022	0.032	0.008
ULI wall	0.16	0.16	0.14	0.23	0.17	0.16	0.08	0.25	0.25	0.07	0.17	0.06
Heart wall	0.043	0.057	0.036	0.024	0.036	0.022	0.020	0.045	0.037	0.025	0.035	0.012
Kidneys	0.083	0.112	0.079	0.036	0.037	0.051	0.021	0.053	0.055	0.035	0.056	0.028
Liver	0.044	0.081	0.074	0.034	0.033	0.027	0.021	0.055	0.043	0.030	0.044	0.020
Lungs	0.028	0.042	0.029	0.019	0.021	0.018	0.018	0.035	0.027	0.019	0.025	0.008
Muscle	0.035	0.035	0.029	0.024	0.027	0.025	0.022	0.038	0.033	0.022	0.029	0.006
Pancreas	0.040	0.044	0.035	0.024	0.029	0.026	0.023	0.043	0.036	0.023	0.032	0.008
Red marrow	0.041	0.049	0.034	0.029	0.035	0.026	0.020	0.046	0.042	0.025	0.035	0.010
Osteogenic cells	0.049	0.053	0.039	0.029	0.037	0.030	0.027	0.052	0.048	0.031	0.039	0.010
Skin	0.024	0.025	0.020	0.015	0.018	0.016	0.015	0.026	0.022	0.015	0.019	0.004
Spleen	0.035	0.055	0.053	0.026	0.025	0.025	0.020	0.035	0.032	0.022	0.033	0.012
Testes	0.039	0.039	0.033	0.029	0.031	0.031	0.027	0.042	-	-	0.034	0.005
Thymus	0.030	0.033	0.024	0.016	0.022	0.018	0.018	0.032	0.026	0.018	0.024	0.006
Thyroid	0.025	0.044	0.022	0.016	0.019	0.016	0.018	0.027	0.021	0.014	0.022	0.009
Total body	0.037	0.039	0.031	0.026	0.028	0.026	0.022	0.041	0.036	0.023	0.031	0.007
UB wall (1 h)	0.25	0.25	0.25	0.26	0.25	0.27	0.24	0.26	0.35	0.35	0.27	0.04
UB wall (2.5 h)	0.58	0.58	0.61	0.69	0.61	0.71	0.61	0.61	0.88	0.95	0.68	0.13
Effective dose (mSv/MBq)	0.097	0.10	0.089	0.11	0.094	0.093	0.061	0.13	0.13	0.072	0.098	0.023

All absorbed dose values are expressed in mGy/MBq. Effective dose is expressed in mSv/MBq [32]. Urinary bladder (UB) wall (*t*) denotes absorbed dose to the bladder wall for a voiding interval of *t*.

PET/CT images were acquired at 6 and 21 h post-administration, and following surgery, the entire surgical specimen was imaged on a microPET scanner. In addition, tumor tissue sections cut from the surgical specimen were exposed to a phosphor imaging plate for up to 7 days for digital autoradiography (DAR). However, not only were the clinical PET scans negative as before, but the *ex vivo* evaluation of the surgical specimen also returned negative results. (Additional file 1: Figure S1 shows the DAR results).

The biodistribution of ^{124}I-IAZGP was characterized by rapid clearance from the blood and whole body primarily via the urinary and, to a lesser extent, GI tracts, with no significant uptake in the parenchymal tissues apart from the salivary glands, presumably reflecting dissociated iodine. In terms of radiation exposure, 148 MBq (4 mCi) of ^{124}I-IAZGP produced absorbed doses to normal parenchymal tissues less than or equal to those produced by typical clinical activities (370 to 444 MBq; 10 to 12 mCi) of ^{18}F-FDG. However, the absorbed doses to the large intestinal and urinary bladder walls were significantly greater for ^{124}I-IAZGP than ^{18}F-FDG. As absorbed doses to the urinary bladder wall depend on the frequency of voiding, study patients were encouraged to hydrate and to void frequently in order to minimize this.

There is no doubt that the use of long-lived positron-emitting nuclides for imaging has intrinsic dosimetric disadvantages compared to short-lived radionuclides, where the balance between image quality and patient dose is usually more favorable. However, the use of a long half-life radionuclide is unavoidable if it takes a long time for sufficient biological contrast to develop; our hypothesis was that PET imaging of tumor hypoxia was such a case. An additional disadvantage associated with ^{124}I is its relatively low positron yield (approximately 24%) coupled with the presence of multiple high-energy

cascade gamma rays which act to further decrease the ratio of PET image quality to patient radiation dose.

We found that PET imaging of ^{124}I-IAZGP in 2D mode was possible up to, at least, 6 to 8 h post-administration and possibly 24 h, although with an enhanced likelihood of low-count reconstruction artifacts. However, imaging at 48 h was generally not feasible with the activities (approximately 148 MBq) and emission times (typically 6 to 8 min per bed position) used in this study. This contrasts to the case where ^{124}I is used to label antibodies with prolonged biological retention, for which clinically useful images may be acquired at times of up to 1 week post-administration [35,36]. This deficiency may be alleviated to some extent by the use of 3D reconstruction methods as long as appropriate corrections are included for cascade coincidences.

However, even with foreseeable improvements in image acquisition and reconstruction methods, our data indicate the uptake of ^{124}I-IAZGP in tumors is insufficient to suggest any clinical role in the management of patients with colorectal or head and neck cancer.

Conclusions

The study reported here is the first trial describing the toxicity and biodistribution of ^{124}I-IAZGP in human subjects. We found that the administration of ^{124}I-IAZGP was safe and that it was rapidly cleared from the body. PET imaging failed to show any differential uptake of ^{124}I-IAZGP in any disease site. While we continue to believe that characterization of tumor hypoxia will be important for individualizing patient treatments, ^{124}I-IAZGP PET in its current form is unlikely to provide any clinical utility for assessing hypoxia in colorectal cancer and head and neck cancer. Despite these negative results with ^{124}I-IAZGP, there is still a strong theoretical rationale for the concept that late PET imaging should provide the most specific indication of tumor hypoxia. It is hoped that new hypoxia agents will emerge, perhaps featuring alternative long-lived positron-emitting radionuclides such as ^{64}Cu, ^{89}Zr, or ^{76}Br, which can provide a convenient way to perform single time-point imaging of tumor hypoxia.

Additional file

Additional file 1: Figure S1. Representative frozen sections from patient surgical specimen showing (left) H&E, (center) digital autoradiogram without digital manipulation, i.e., each section is quantitatively comparable, and (right) digital autoradiogram optimized to maximize contrast. The exposure time for the autoradiograms was 4 days. Overall, the absolute amount of ^{124}I in the tumor is low (compare signal/background in center) and relatively uniform with no enhancement in tumor uptake compared to normal colon.

Competing interests

The authors declare that they have no competing interests.

Authors' contributions

JAOD, JGG, HS, NYL, CRD, JLH, PBZ, and CCL participated in the concept, design, and analysis of the study. JAOD, JLH, SDC, and PBZ acquired the data. JGG, NYL, JAR, SALK, and TL were responsible for primary clinical management and patient accrual. EMB and SC participated in radiotracer development, formulation, and quality assurance. JAOD and JAR drafted the manuscript. All authors read and approved the final manuscript.

Acknowledgments

We are grateful to Richard F Schneider and J Donald Chapman, formerly of Fox Chase Cancer Center, Philadelphia, PA, USA, for scientific advice and providing the IAZGP precursor; Ron Finn, Jacek Koziorowski, Ouathek Ouerfelli, James Russell, and Makiko Suehiro for developmental radiochemistry and assistance with the IND submission; Ernest Flatts, Andrew Nagel, Shutian Ruan, and Alex Wills for research support; Rachel Levy for editorial assistance; Amabella Lindo and Susan Reyes for nursing care; Howard Sheh and Jason Lewis for cyclotron production of ^{124}I. This work was supported by the following NIH grants: P01 CA115675 (CC Ling), RO1 CA82534 (JG Guillem), R24 CA83084 (Small-Animal Imaging Research Program), and P30 CA08748 (Center Grant).

Author details

[1]Department of Medical Physics, Memorial Sloan-Kettering Cancer Center, New York, NY 10065, USA. [2]Department of Surgery, Memorial Sloan-Kettering Cancer Center, New York, NY 10065, USA. [3]Department of Radiology, Memorial Sloan-Kettering Cancer Center, New York, NY 10065, USA. [4]Department of Radiation Oncology, Memorial Sloan-Kettering Cancer Center, New York, NY 10065, USA. [5]Department of Radiology, Columbia University Medical Center, New YorkNY 10027, USA. [6]Department of Surgery, Columbia University Medical Center, New York, NY 10027, USA. [7]Department of General and Visceral Surgery, Robert-Bosch Hospital, Stuttgart 70376, Germany.

Received: 18 March 2013 Accepted: 8 April 2013
Published: 3 June 2013

References

1. Moeller BJ, Richardson RA, Dewhirst MW: **Hypoxia and radiotherapy: opportunities for improved outcomes in cancer treatment.** *Cancer Metastasis Rev* 2007, **26:**241–248.
2. Brahimi-Horn MC, Chiche J, Pouyssegur J: **Hypoxia and cancer.** *J Mol Med* 2007, **85:**1301–1307.
3. Liao D, Johnson RS: **Hypoxia: a key regulator of angiogenesis in cancer.** *Cancer Metastasis Rev* 2007, **26:**281–290.
4. Bertout JA, Patel SA, Simon MC: **The impact of O2 availability on human cancer.** *Nat Rev Cancer* 2008, **8:**967–975.
5. Bristow RG, Hill RP: **Hypoxia, DNA repair and genetic instability.** *Nat Rev Cancer* 2008, **8:**180–192.
6. Dewhirst MW, Cao Y, Moeller B: **Cycling hypoxia and free radicals regulate angiogenesis and radiotherapy response.** *Nat Rev Cancer* 2008, **8:**425–437.
7. Lunt SJ, Chaudary N, Hill RP: **The tumor microenvironment and metastatic disease.** *Clin Exp Metastasis* 2009, **26:**19–34.
8. Pires IM, Bencokova Z, Milani M, Folkes LK, Li J-L, Stratford MR, Harris AL, Hammond EM: **Effects of acute versus chronic hypoxia on DNA damage responses and genomic instability.** *Cancer Res* 2010, **70:**925–935.
9. Nordsmark M, Bentzen SM, Rudat V, Brizel D, Lartigau E, Stadler P, Becker A, Adam M, Molls M, Dunst J, Terriis DJ, Overgaard J: **Prognostic value of tumor oxygenation in 397 head and neck tumors after primary radiation therapy. An international multi-center study.** *Radiother Oncol* 2005, **77:**18–24.
10. Hockel M, Schlenger K, Aral B, Mitze M, Schaffer U, Vaupel P: **Association between tumor hypoxia and malignant progression in advanced cancer of the uterine cervix.** *Cancer Res* 1996, **56:**4509–4515.
11. Fyles A, Milosevic M, Pintilie M, Syed A, Levin W, Manchul L, Hill RP: **Long-term performance of interstial fluid pressure and hypoxia as prognostic factors in cervix cancer.** *Radiother Oncol* 2006, **80:**132–137.
12. Rasey JS, Koh WJ, Evans ML, Peterson LM, Lewellen TK, Graham MM, Krohn KA: **Quantifying regional hypoxia in human tumors with positron emission tomography of [18F]fluoromisonidazole: a pretherapy study of 37 patients.** *Int J Radiat Oncol Biol Phys* 1996, **36:**417–428.
13. Rajendran JG, Wilson DC, Conrad EU, Peterson LM, Bruckner JD, Rasey JS, Chin LK, Hofstrand PD, Grierson JR, Eary JF, Krohn KA: **[(18)F]FMISO and**

[(18)F]FDG PET imaging in soft tissue sarcomas: correlation of hypoxia, metabolism and VEGF expression. *Eur J Nucl Med Mol Imaging* 2003, **30:**695–704.
14. Postema EJ, McEwan AJ, Riauka TA, Kumar P, Richmond DA, Abrams DN, Wiebe LI: **Initial results of hypoxia imaging using 1-alpha-D: -(5-deoxy-5-[18F]-fluoroarabinofuranosyl)-2-nitroimidazole (18F-FAZA).** *Eur J Nucl Med Mol Imaging* 2009, **36:**1565–1573.
15. Garcia-Parra R, Wood D, Shah RB, Siddiqui J, Hussain H, Park H, Desmond T, Meyer C, Piert M: **Investigation on tumor hypoxia in resectable primary prostate cancer as demonstrated by 18F-FAZA PET/CT utilizing multimodality fusion techniques.** *Eur J Nucl Med Mol Imaging* 2011, **38:**1816–1823.
16. Dolbier WR Jr, Li AR, Koch CJ, Shiue CY, Kachur AV: **[18F]-EF5, a marker for PET detection of hypoxia: synthesis of precursor and a new fluorination procedure.** *App Radiat Isot* 2001, **54:**73–80.
17. Komar G, Seppanen M, Eskola O, Lindholm P, Gronroos TJ, Forsback S, Sipila H, Evans SM, Solin O, Minn H: **18F-EF5: a new PET tracer for imaging hypoxia in head and neck cancer.** *J Nucl Med* 2008, **49:**1944–1951.
18. Lehtio K, Eskola O, Viljanen T, Oikonen V, Gronroos T, Sillanmaki L, Grenman R, Minn H: **Imaging perfusion and hypoxia with PET to predict radiotherapy response in head-and-neck cancer.** *Int J Radiat Oncol Biol Phys* 2004, **59:**971–982.
19. Yue J, Yang Y, Cabrera AR, Sun X, Zhao S, Xie P, Zheng J, Ma L, Fu Z, Yu J: **Measuring tumor hypoxia with (1)(8)F-FETNIM PET in esophageal squamous cell carcinoma: a pilot clinical study.** *Dis Esophagus* 2012, **25:**54–61.
20. Lewis JS, Laforest R, Dehdashti F, Grigsby PW, Welch MJ, Siegel BA: **An imaging comparison of 64Cu-ATSM and 60Cu-ATSM in cancer of the uterine cervix.** *J Nucl Med* 2008, **49:**1177–1182.
21. *Copper Cu 64-ATSM and PET/CT scan in predicting disease progression in patients with newly-diagnosed stage IB, stage II, stage III, or stage IVA cervical cancer who are undergoing chemoradiotherapy per NCCN guidelines (ACRIN 6682).* http://clinicaltrials.gov/ct2/show/NCT00794339.
22. Dehdashti F, Grigsby PW, Lewis JS, Laforest R, Siegel BA, Welch MJ: **Assessing tumor hypoxia in cervical cancer by PET with 60Cu-labeled diacetyl-bis(N4-methylthiosemicarbazone).** *J Nucl Med* 2008, **49:**201–205.
23. Minagawa Y, Shizukuishi K, Koike I, Horiuchi C, Watanuki K, Hata M, Omura M, Odagiri K, Tohnai I, Inoue T, Tateishi U: **Assessment of tumor hypoxia by Cu-62-ATSM PET/CT as a predictor of response in head and neck cancer: a pilot study.** *Ann Nucl Med* 2011, **25:**339–345.
24. Thorwarth D, Eschmann SM, Scheiderbauer J, Paulsen F, Alber M: **Kinetic analysis of dynamic 18F-fluoromisonidazole PET correlates with radiation treatment outcome in head-and-neck cancer.** *BMC Cancer* 2005, **5:**152.
25. Wang WL, Lee NY, Georgi JC, Narayanan M, Guillem J, Schoder H, Humm JL: **Pharmacokinetic analysis of hypoxia F-18-fluoromisonidazole dynamic PET in head and neck cancer.** *J Nucl Med* 2010, **51:**37–45.
26. Schneider RF, Engelhardt EL, Stobbe CC, Fenning MC, Chapman JD: **The synthesis and radiolabelling of novel markers of tissue hypoxia of the iodinated azomycin nucleoside class.** *J Labelled Comp Radiopharm* 1997, **39:**541–557.
27. Zanzonico P, O'Donoghue J, Chapman JD, Schneider R, Cai S, Larson S, Wen B, Chen Y, Finn R, Ruan S, Gerweck L, Humm J, Ling C: **Iodine-124-labeled iodo-azomycin-galactoside imaging of tumor hypoxia in mice with serial microPET scanning.** *Eur J Nucl Med Mol Imaging* 2004, **31:**117–128.
28. Riedl CC, Brader P, Zanzonico PB, Chun YS, Woo Y, Singh P, Carlin S, Wen B, Ling CC, Hricak H, Fong Y: **Imaging hypoxia in orthotopic rat liver tumors with iodine 124-labeled iodoazomycin galactopyranoside PET.** *Radiology* 2008, **248:**561–570.
29. Stabin MG, Sparks RB, Crowe E: **OLINDA/EXM: the second-generation personal computer software for internal dose assessment in nuclear medicine.** *J Nucl Med* 2005, **46:**1023–1027.
30. ICRP: **Limits for intakes of radionuclides by workers. ICRP publication 30 (part 1).** *Ann ICRP* 1979, **2:**3–4.
31. ICRP: **Basic anatomical and physiological data for use in radiological protection reference values. ICRP publication 89.** *Ann ICRP* 2002, **32:**3–4.
32. ICRP: **1990 Recommendations of the International Commission on Radiological Protection. ICRP publication 60.** *Ann ICRP* 1991, **21:**1–3.
33. Suehiro M, Burgman P, Carlin S, Burke S, Yang GB, Ouerfelli O, Oehler-Janne C, O'Donoghue J, Ling C, Humm J: **Radiosynthesis of I-131 IAZGP via nucleophilic substitution and its biological evaluation as a hypoxia marker - is specific activity a factor influencing hypoxia-mapping ability of a hypoxia marker?** *Nucl Med Biol* 2009, **36:**477–487.
34. Li XF, Sun XR, Ma YY, Suehiro M, Zhang MT, Russell J, Humm JL, Ling CC, O'Donoghue JA: **Detection of hypoxia in microscopic tumors using I-131-labeled iodo-azomycin galactopyranoside (I-131-IAZGP) digital autoradiography.** *Eur J Nucl Med Mol Imaging* 2010, **37:**339–348.
35. Divgi CR, Pandit-Taskar N, Jungbluth AA, Reuter VE, Gonen M, Ruan S, Pierre C, Nagel A, Pryma DA, Humm J, Larson SM, Old LJ, Russo P: **Preoperative characterisation of clear-cell renal carcinoma using iodine-124-labelled antibody chimeric G250 (124I-cG250) and PET in patients with renal masses: a phase I trial.** *Lancet Oncol* 2007, **8:**304–310.
36. Carrasquillo JA, Pandit-Taskar N, O'Donoghue JA, Humm JL, Zanzonico P, Smith-Jones PM, Divgi CR, Pryma DA, Ruan S, Kemeny NE, Fong Y, Wong D, Jaggi JS, Scheinberg DA, Gonen M, Panageas KS, Ritter G, Jungbluth AA, Old LJ, Larson SM: **(124)I-huA33 antibody PET of colorectal cancer.** *J Nucl Med* 2011, **52:**1173–1180.

doi:10.1186/2191-219X-3-42
Cite this article as: O'Donoghue *et al.*: Pilot study of PET imaging of ^{124}I-iodoazomycin galactopyranoside (IAZGP), a putative hypoxia imaging agent, in patients with colorectal cancer and head and neck cancer. *EJNMMI Research* 2013 **3**:42.